Biomedicine & Pharmacotherapy 193 (2025) 118757

Contents lists available at ScienceDirect

Biomedicine & Pharmacotherapy

journal homepage: www.elsevier.com/locate/biopha

Apremilast attenuates hepatic steatosis and metabolic dysfunction in a murine model of MASLD: Implications for patients with Psoriatic disease

Miriam Ruiz-Ponce [a,1], Sergio Rodriguez-Cuenca [b,c,*,1], Jesus Eduardo Martin-Salazar [a], Carlos Pérez-Sánchez [a,d,e], Julio M. Martínez-Moreno [d], Adrián Llamas-Urbano [d], Mark Campbell [b,c], Laura Romero-Zurita [a], Maria Dolores López-Montilla [a], Laura Cuesta-López [a], Antonio Manuel Barranco [a], Pedro Ortiz-Buitrago [a], Chary López-Pedrera [a], Alejandro Escudero-Contreras [a], Eduardo Collantes-Estevez [a], Clementina López-Medina [a], Antonio Vidal-Puig [b,c,1], Iván Arias-de la Rosa [f,g,h,1], Nuria Barbarroja [a,d,*,1]

[a] *Rheumatology Service/Department of Medical and Surgical Sciences, Maimonides Institute for Research in Biomedicine of Cordoba (IMIBIC), University of Cordoba, Reina Sofia University Hospital, Córdoba, Spain*
[b] *Wellcome-MRC Institute of Metabolic Science and MRC Metabolic Diseases Unit, University of Cambridge, Cambridge, UK*
[c] *Cambridge University Nanjing Centre of Technology and Innovation, Nanjing, PR China*
[d] *Cobiomic Bioscience S.L, Córdoba, Spain*
[e] *Department of Cell Biology, Physiology and Immunology, Maimonides Institute of Biomedical Research of Cordoba (IMIBIC), Reina Sofia University Hospital, University of Córdoba, , Córdoba, Spain*
[f] *Gastroenterology, General Hospital of Tomelloso, Tomelloso, Spain*
[g] *Institute of Health Research of Castilla-La Mancha (IDISCAM), Toledo, Spain*
[h] *Biomedical Research Network Centre for Liver and Digestive Diseases (CIBERehd), Madrid, Spain*

A R T I C L E I N F O

Keywords:
Metabolic dysfunction-associated steatotic liver disease (MASLD)
Psoriatic Disease (PsD)
Psoriasis (PsO)
Apremilast
PDE4 inhibitor
mouse model
Gan diet
hepatic steatosis
proteomics
Olink

A B S T R A C T

Background: Metabolic dysfunction-associated steatotic liver disease (MASLD) is a major cause of morbidity, linked to obesity, type 2 diabetes, and cardiovascular disease. Psoriatic disease (PsD), a chronic inflammatory condition, often coexists with MASLD, exacerbating systemic inflammation and cardiometabolic risk. Apremilast, a selective PDE4 inhibitor approved for PsD, may provide additional metabolic benefits by improving weight, lipid metabolism, and insulin sensitivity.
Objective: To evaluate the effects of apremilast on metabolic dysfunction, hepatic steatosis, and systemic inflammation in PsD patients with metabolic comorbidities, and to investigate mechanistic impact in a murine model of diet-induced MASLD.
Methods: Twenty PsD patients treated with apremilast were stratified by metabolic comorbidities. Glucose metabolism and liver function were monitored for 6 months. In parallel, C57BL/6 J mice were fed chow or GAN diet. After 14 weeks, apremilast (10 mg/kg/day) was administered for two weeks. Body weight, adiposity, liver biomarkers, insulin resistance, histology, and proteomics were evaluated.
Results: In PsD patients with comorbidities, apremilast reduced fasting insulin, HOMA-IR, transaminases, and the hepatic steatosis index. GAN-fed mice developed steatosis, increased fat mass, and elevated alanine

Abbreviations: NAFLD, non-alcoholic fatty liver disease; DM2, type 2 diabetes; HTA, hypertension; MetS, metabolic syndrome; NASH, non-alcoholic steatohepatitis; CVD, cardiovascular disease; MASLD, Metabolic dysfunction-associated steatotic liver disease; PsA, psoriatic arthritis; Pso, psoriasis; PDE4, phosphodiesterase 4; HDL, high Density Lipoprotein; MTX, methotrexate; IR, insulin resistance; BMI, body mass index; H&E, Hematoxylin and eosin; PSR, picrosirius Red; PEA, proximity extension assay; ALT, alanine aminotransferase; AST, aspartate aminotransferase; HOMA-IR, homeostatic model assessment for insulin resistance; MWAT, mesenteric adipose tissue; IWAT, inguinal adipose tissue; EWAT, epididymal adipose tissue; GAN diet, Gubra-Amylin NASH diet; CHOW diet, standard chow diet; PCR, polymerase chain reaction; SPLSDA, Sparse Partial Least Squares Discriminant Analysis; LDL, low-Density Lipoprotein; HbA1c, Glycated Hemoglobin A1c; PsD, Psoriatic Disease; DAPSA, the Disease Activity in Psoriatic Arthritis; TG, triglycerides.

* Correspondence to: GC-05 Group, second floor, IMIBIC, Avda. Menendez Pidal s/n, Córdoba 14004, Spain.
E-mail addresses: sr441@medschl.cam.ac.uk (S. Rodriguez-Cuenca), b52bapun@uco.es (N. Barbarroja).
[1] These authors contributed equally to this work

https://doi.org/10.1016/j.biopha.2025.118757
Received 27 September 2025; Received in revised form 30 October 2025; Accepted 7 November 2025
Available online 12 November 2025

aminotransferase (ALT) and HOMA-IR levels. Apremilast reduced body weight, ALT, insulin resistance, and hepatic fat. Histology confirmed a decrease in fibrosis. Proteomic profiling showed modulation of inflammatory, fibrotic, and lipid metabolic pathways, partially reversing GAN-induced proinflammatory signatures in liver, adipose tissue, and muscle.

Conclusions: Apremilast ameliorates hepatic dysfunction, improves insulin sensitivity, and reduces systemic metabolic dysfunction in a murine MASLD model. These findings support its therapeutic potential in PsD patients with metabolic disease, offering both anti-inflammatory and metabolic benefits.

1. Introduction

Liver disease represents one of the leading causes of morbidity and mortality worldwide [1,2]. A meta-analysis of studies conducted between 2006 and 2014 estimated a 25.3 % prevalence of NAFLD in the general population, mostly based on studies in Western populations. Meanwhile, a study published in 2023 reported a 38 % prevalence of hepatic steatosis in the general population [3]. In 2023, the term NAFLD was proposed to be replaced with MASLD (Metabolic dysfunction-associated steatotic liver disease), acknowledging that the excessive accumulation of fat in the liver is closely linked to the presence of at least one cardiometabolic risk factor, in the absence of harmful alcohol intake [4]. Over the course of its clinical progression, MASLD goes through various stages. The first sign of liver damage is steatosis characterized by the excessive accumulation of lipids in hepatocytes. This condition may progress into inflammatory processes, early and advance fibrosis, and in its more advanced stages, leading to cirrhosis or hepatocellular carcinoma [5]. Metabolic comorbidities frequently associated with this disease include obesity, type 2 diabetes (DM2), hyperlipidaemia, hypertension (HTA), and metabolic syndrome (MetS). In the recent years, a growing body of evidence suggests that patients with Psoriatic Disease (PsD) including psoriatic arthritis (PsA) and Psoriasis (PsO), present a higher prevalence of liver dysfunction compared to the general population. In these patients, hepatic steatosis can be considered an extra-articular manifestation, reflecting a connection between systemic inflammation and the metabolic comorbidities associated with this condition. Its presence is associated with greater clinical activity and deterioration of the cardiovascular profile [6–9].

Our research group has recently shown that the increased risk of hepatic steatosis and fibrosis in PsA patients is not only linked to cardiometabolic comorbidities but also to disease-specific factors like psoriasis, onychopathy, and systemic inflammation, independently of methotrexate use. In addition, we observed that targeted therapies such as anti-JAK or anti-PDE-4 may offer promising benefits for PsA patients with liver dysfunction [10]. Therefore, since cardiometabolic comorbidities are highly prevalent in MetS, it is reasonable to expect that hepatic steatosis further increases cardiovascular risk in patients with PsA, which is the leading cause of morbidity and mortality in these patients.

The therapeutic approach against PsD includes drugs that not only control inflammatory activity and psoriasis but may also have beneficial effects on associated comorbidities. Apremilast, a selective phosphodiesterase 4 (PDE4) inhibitor, reduces the production of proinflammatory cytokines involved in the pathophysiology of PsD [11] and it has shown promising results on reducing cardiovascular risk factors in patients with psoriatic disease, including improvements in body weight, fat distribution, lipid profiles and insulin sensitivity [11,12], providing metabolic and anti-inflammatory benefits in patients with PsD.

In this study, we first analyzed a real-world cohort of patients with PsA treated with apremilast, identifying two distinct subgroups based on their metabolic profile. Patients with higher metabolic burden—including obesity, insulin resistance, and features of metabolic syndrome—exhibited significant improvements in glycemic control and liver function markers after six months of treatment, including reductions in fasting glucose, insulin, HOMA-IR, transaminases, and hepatic steatosis index (HSI). These findings suggested that apremilast may exert beneficial metabolic and hepatic effects in addition to its known anti-inflammatory properties. To investigate further the underlying mechanisms of these clinical observations, we designed a preclinical model to test the efficacy of apremilast on inflammatory markers of MASLD using a diet induced model of fatty liver disease.

Our results provide evidence that the use of apremilast could help mitigating the severity of the inflammatory signature observed in MASLD and reduce associated cardiovascular risk in PSD patients. For this purpose, we designed a preclinical model to test the efficacy of apremilast on inflammatory markers of MASLD using a diet induced model of fatty liver disease.

2. Methods

2.1. PsA patients and data collection

Clinical data from 20 PsA patients, previously included in a study published by our group [12], were analyzed. All patients met the CASPAR classification criteria for psoriatic arthritis and were recruited at the Rheumatology Departments of Reina Sofía Hospital in Córdoba, Spain [13]. The cohort included both men and women in similar proportions; specifically, 9 patients were women, and 6 of them (66.6 %) were postmenopausal, as recorded during data collection.

Of these, nine patients received apremilast monotherapy (60 mg/day), while the remaining eleven were treated with a combination of methotrexate (13.50 ± 3.57 mg/week) and apremilast (60 mg/day). Data was collected at baseline and after 6 months of apremilast treatment.

All patients successfully completed the required questionnaires assessing healthy lifestyle factors as well as disease activity, specifically the Disease Activity in Psoriatic Arthritis (DAPSA) score and visual analogue scale. The DAPSA score was calculated as the sum of tender joint count (out of 68 joints), swollen joint count (out of 66 joints), patient global assessment, patient pain assessment (both on a 0–10 cm visual analogue scale), and C-reactive protein level (mg/dL) [14].

Laboratory parameters including fasting insulin, glucose, and liver enzymes (aspartate aminotransferase [AST] and alanine aminotransferase [ALT]) were recorded. The homeostasis model assessment of insulin resistance (HOMA-IR) was calculated using the following standardized formula:

HOMA-IR = [fasting insulin (μU/mL) × fasting glucose (mg/dL)] / 405

Body mass index (BMI) was calculated as:

$BMI = \text{weight (kg)} / \text{height (m)}^2$

Obesity was defined as BMI > 30 kg/m^2.

Metabolic syndrome was diagnosed in patients meeting at least three of the following conditions according to the National Cholesterol Education Program Adult Treatment Panel III (NCEP ATP III) criteria: abdominal obesity (men > 102 cm; women > 88 cm), triglycerides (TG) > 150 mg/dL, HDL (men < 40 mg/dL; women < 50 mg/dL), blood pressure > 130/85 mmHg, and glucose levels > 110 mg/dL [15]. *The Hepatic Steatosis Index (HSI)* was calculated to estimate the presence of NAFLD using the following validated formula:

HSI = 8 × (ALT / AST) + BMI + 2 (if female) + 2 (if type 2 diabetes mellitus is present)

Clustering: To distinguish patient phenotypes based on the concomitant presence of cardiometabolic comorbidities, an unsupervised clustering analysis was conducted using a hard-clustering approach.

2.2. Animals and experimental design

A total of 32 male C57BL/6 J wild-type mice were used for this study, which was conducted under the regulations of the Animals (Scientific Procedures) Act 1986 Amendment Regulations 2012, following ethical review by the University of Cambridge Animal Welfare and Ethical Review Body (AWERB). The mice were housed under pathogen-free conditions according to UK Home Office guidelines and maintained by the Disease Model Core unit. They were kept in a temperature-controlled room (22°C) with a 12-hour light/dark cycle and 55 % relative humidity, with ad libitum access to food and water. The animals were divided into two dietary groups: 16 mice were assigned to the CHOW diet, a standard diet (DS-105, Safe Diets) consisting of 64.3 % carbohydrate, 22.4 % protein, and 13.3 % lipid of total calories, serving as the control group, while the remaining 16 mice were placed on the GAN diet, a high-fat diet (20 % carbohydrate, 20 % protein, 60 % lipid) used to model NAFLD. Within each dietary group, mice were further subdivided into two treatment groups of eight animals each, with one subgroup receiving vehicle treatment as the control, and the other administered apremilast (10 mg/kg per day). The study lasted 16 weeks, with dietary intervention starting at week 0, hepatic steatosis induced in the GAN diet group, and apremilast treatment initiated at week 14.

2.3. Treatment administration

Apremilast was administered daily via oral gavage (10 mg/kg per day) from week 14 to week 16, using 0.5 % carboxymethyl/0.25 % Tween 80 in sterile water as vehicle. The control group received an equivalent volume of vehicle based on body weight.

2.4. Monitoring and measurements

2.4.1. Body weight, body composition, and food intake analysis

The impact of the treatment on body weight, fat mass percentage, and lean mass was monitored and evaluated throughout the study. Mice were weighed weekly, with daily weight monitoring from week 14 to week 16. Lean and fat mass composition was assessed using a body composition analyzer. Additionally, food intake was monitored daily starting from the administration of apremilast, with the total amount of food consumed per cage recorded and normalized per mouse.

2.4.2. Tissue collection

At the end of the experimental period, mice were sacrificed via cervical dislocation. Tissue samples, including liver, serum, and metabolic tissues (epididymal, inguinal, mesenteric adipose tissue and gastrocnemius muscle), were collected and weighed. Samples were stored at −80°C for molecular analyses or fixed in 10 % buffered formalin for histopathology analysis.

2.4.3. Blood collection

Blood samples were collected, and plasma levels of alanine aminotransferase (ALT), aspartate aminotransferase (AST), glucose, and insulin were measured to assess liver function and metabolic status.

2.5. Histological and immunohistochemical analysis

Liver samples were processed for immunohistochemistry and histological staining. Hematoxylin and eosin (H&E) staining was used to evaluate general liver morphology, with particular attention to fat infiltration (steatosis). Steatosis was assessed by identifying and quantifying lipid droplet accumulation within hepatocytes. The percentage of lipid droplets was calculated as: lipid droplet area/liver area× 100. All regions of interest (ROIs) analyzed were of equal size, and for each sample, the total lipid droplet area was obtained by summing the measurements from the ten ROIs. Additionally, hepatocellular injury and fibrosis were evaluated using Picrosirius Red (PSR) staining, which specifically highlights collagen deposition, allowing for the assessment of hepatic fibrosis. The percentage of fibrosis was calculated using the formula: fibrosis area/liver area× 100. Image analysis was performed using Fiji software (version 1.54p; Fiji Is Just ImageJ, NIH, Maryland, USA). Custom macros were developed to automate and standardize the quantification of fibrosis and steatosis. For each sample, ten randomly selected regions of interest (ROIs) were analyzed to quantify both the number and area of lipid droplets.

2.6. Assessment of insulin resistance

Insulin resistance (IR) was evaluated using the homeostasis model assessment (HOMA-IR), based on fasting levels of glucose and insulin. The HOMA-IR index was calculated according to the formula: fasting glucose (mmol/L) × fasting insulin (μU/mL) / 22.5, as previously described [16].

2.7. Protein expression analysis

Proteins were extracted from metabolic tissues, including eWAT, liver and skeletal muscle. Tissues were homogenized in radioimmunoprecipitation assay (RIPA) buffer containing 50 mM Tris-HCl, 150 mM NaCl, 1 mM EDTA, 1 % Triton X-100 and 0.4 % sodium deoxycholate at pH 7.4. Homogenization was performed using a Retsch MM400 steel ball mill (Retsch, Germany) for 2 min at 25 s^{-1} . The homogenates were then centrifuged at 10000xg for 15 min at 4ºC to separate protein extracts, which were collected from the supernatant, transferred to clean tubes, and stored at −80ºC until further analysis. Protein concentration was quantified using the Bradford assay. For serum samples, 1 μL of sample was used directly for protein expression analysis without prior extraction.

The expression of 92 proteins involved in inflammation, lipid metabolism, and glucose metabolism was analyzed using the Olink Target 96 Mouse Exploratory panel (Cobiomic Bioscience S.L, Córdoba, Spain), employing proximity extension assay (PEA) technology. This highly sensitive and specific method uses pairs of antibodies, each conjugated to unique, complementary DNA oligonucleotides. When both antibodies bind simultaneously to their target protein, the oligonucleotides are brought into close proximity and can hybridize. This hybridization enables a DNA polymerase to extend and form a new PCR target sequence, which is subsequently amplified and quantified using high-throughput real-time PCR. The results obtained from the proximity extension assay were expressed in Normalized Protein eXpression (NPX) units, which are relative, log2-scaled values that reflect protein abundance. Protein detectability varied depending on the tissue analyzed, with the following percentages of proteins detected above the assay's limit of detection (LOD): serum 96.74 %, liver 84.78 %, eWAT 92.39 % and muscle 84.78 %.

2.8. Enrichment analysis and functional characterization of proteins

Proteins with a Spearman correlation coefficient $|r| > 0.60$ and a p-value < 0.001 were selected for functional analysis. Mouse proteins were first mapped to their human orthologs using Ensembl's BioMart tool to ensure compatibility with human-based annotation resources. Functional enrichment analysis was performed using Enrichr and Enrichr-KG (Icahn School of Medicine at Mount Sinai), which integrate multiple databases including Gene Ontology (GO), KEGG, and Reactome. Enrichment results were filtered and ranked based on combined scores and adjusted p-values (FDR$<$ 0.05). Visualization of enriched terms and functional categories was carried out using R (version 4.3.2), employing appropriate packages for plotting enrichment results and

summarizing the data.

To further investigate the biological roles, tissue-specific expression, and disease associations of the selected proteins, we consulted The Human Protein Atlas, GeneCards, and UniProt databases. These resources provided detailed annotations on protein localization, functional domains, expression patterns, and known involvement in physiological and pathological processes.

2.9. Statistical analysis

The normal distribution of each variable was analyzed. For comparisons between two independent groups, Student's unpaired *t*-test was used for parametric data, while the Mann-Whitney rank sum test was used for non-parametric data. For multiple comparisons, one-way or two-way ANOVA was used for normally distributed data, as appropriate, and the Kruskal-Wallis test was applied for non-parametric data. Spearman's correlation coefficients were calculated to evaluate associations between clinical and biochemical variables and protein expression levels. In addition, linear regression analyses were performed to further assess the relationships between selected variables and to approximate potential dependency patterns among them. Data were expressed as mean ± standard deviation (SD). A *p*-value $p < 0.05$ was considered statistically significant. Protein expression data were analyzed using bioinformatics tools, including Python-based scripts and MetaboAnalyst. In MetaboAnalyst, sparse Partial Squares Discriminant Analysis (sPLS-DA) and loading plots were performed to identify the proteins that most strongly contributed to the separation between experimental groups. Graphs and data visualizations were generated using GraphPad Prism (version 9.0.1), R (version 4.3.2), and Python.

3. Results

3.1. Apremilast improves metabolic and hepatic parameters in a subgroup of psoriatic arthritis patients with metabolic comorbidities

We analyzed a real-world cohort of 20 patients with PsA treated with apremilast. Patients were stratified using supervised clustering based on the presence of metabolic comorbidities, which identified two distinct clinical subgroups. Clinical details of the patients included in the two clusters are described in Fig. 1A. Cluster 1 (n = 12) was composed of patients with low metabolic burden, showing mild signs of insulin resistance, while Cluster 2 (n = 8), was enriched in individuals with features of metabolic dysfunction, including obesity, hypertension, insulin resistance and metabolic syndrome, and thus possibly suspected hepatic steatosis (Fig. 1B). We examined the effect of 6 months of apremilast treatment on glycemic control and liver function, including fasting glucose, insulin, HOMA-IR, ALT, AST, and the hepatic steatosis index (HSI). Patients in Cluster 2 exhibited a significant improvement, reducing fasting glucose, insulin, and HOMA-IR (Fig. 1C), indicating improved insulin sensitivity, and also decreased ALT, AST, and HSI, reflecting a potential amelioration of hepatic involvement (Fig. 1D). In contrast, Cluster 1 patients showed no significant changes, consistent with their low baseline metabolic involvement.

3.2. Apremilast ameliorates GAN Diet-induced metabolic and hepatic alterations in mice

In our preclinical design, the use of GAN diet induced significant metabolic changes in mice compared to chow fed mice. A progressive increase in body weight was observed in the GAN group over time (Fig. 2A). This increase was associated with a marked increase in fat

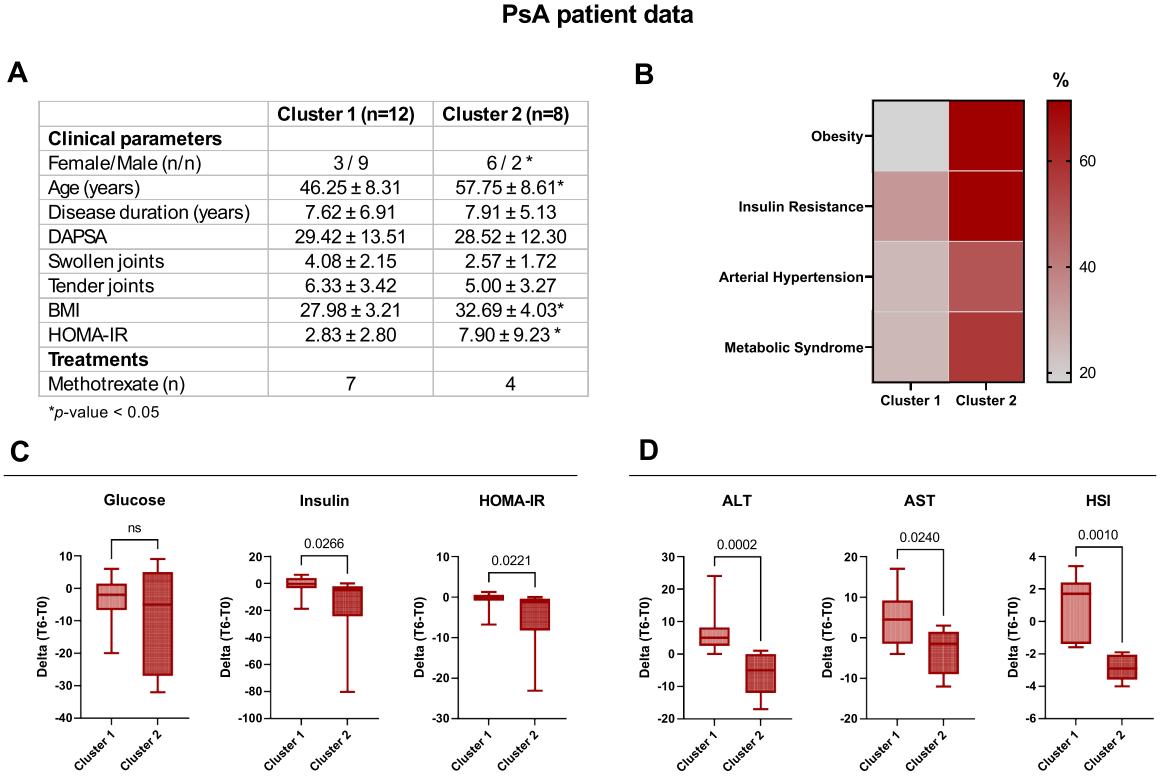

	Cluster 1 (n=12)	Cluster 2 (n=8)
Clinical parameters		
Female/Male (n/n)	3 / 9	6 / 2 *
Age (years)	46.25 ± 8.31	57.75 ± 8.61*
Disease duration (years)	7.62 ± 6.91	7.91 ± 5.13
DAPSA	29.42 ± 13.51	28.52 ± 12.30
Swollen joints	4.08 ± 2.15	2.57 ± 1.72
Tender joints	6.33 ± 3.42	5.00 ± 3.27
BMI	27.98 ± 3.21	32.69 ± 4.03*
HOMA-IR	2.83 ± 2.80	7.90 ± 9.23 *
Treatments		
Methotrexate (n)	7	4

*p-value < 0.05

Fig. 1. Metabolic and hepatic effects of Apremilast in PsA patients. (A) Descriptive clinical data of PsA patients included in the two clusters at treatment initiation. (B) Prevalence of comorbidities in cluster 1 and 2. (C) Significant differences in the variation of glycemic parameters after six months of treatment between the two clusters. (D) Significant differences in the variation of hepatic parameters after six months of treatment between the two clusters. DAPSA, Disease Activity in Psoriatic Arthritis score; BMI, Body Mass Index; HOMA-IR, Homeostatic Model Assessment for Insulin Resistance; ALT, Alanine Transaminase; AST, Aspartate Transaminase; HSI, Hepatic Steatosis Index.

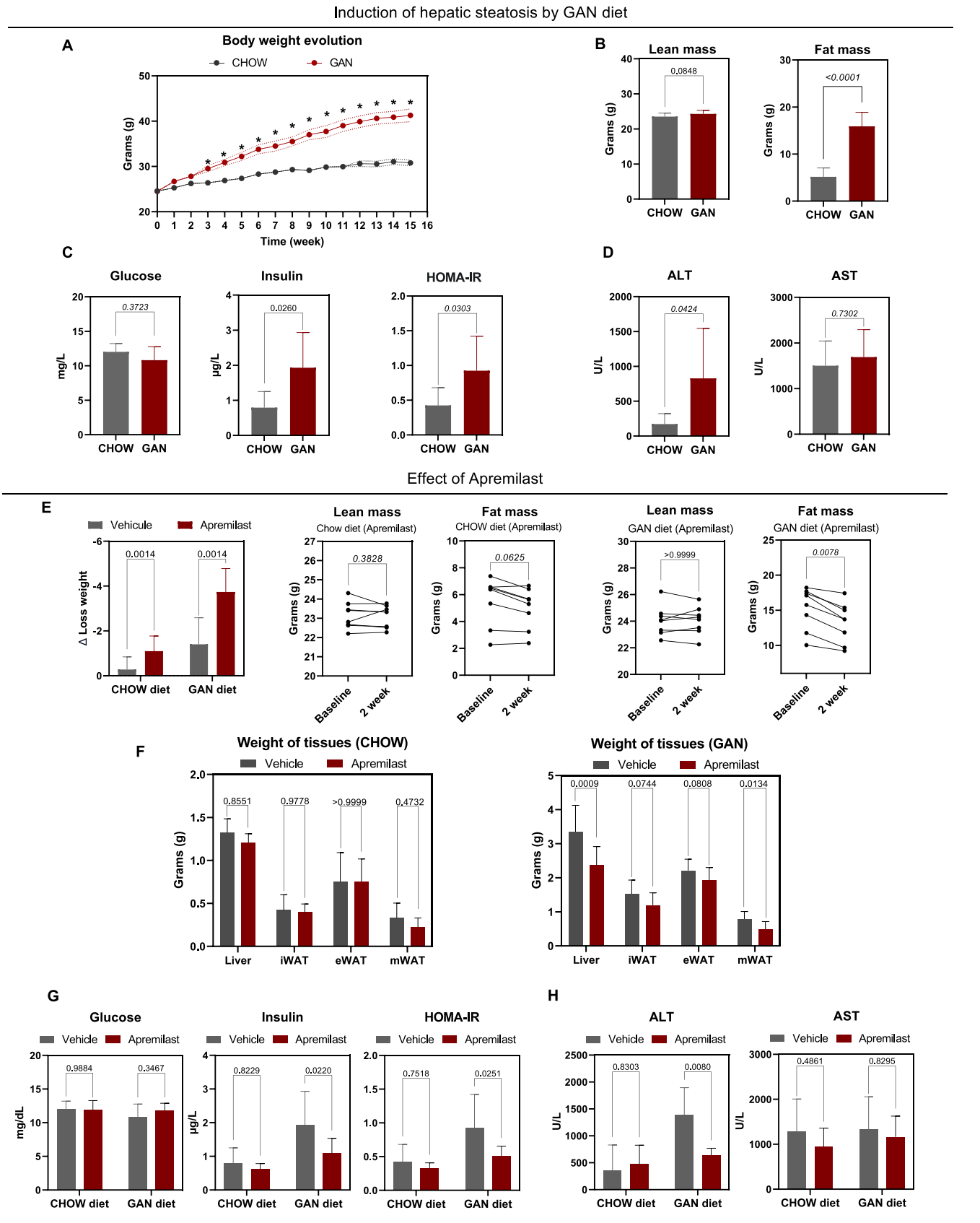

(caption on next page)

Fig. 2. Induction of hepatic steatosis by GAN diet and the effects of Apremilast treatment. (A) Body weight evolution (grams) over time (weeks) in mice fed with standard CHOW diet *versus* GAN diet. (B) Lean mass and fat mass (grams) measured at baseline in CHOW and GAN mice. (C) Circulating glucose (mg/dL), insulin (μg/L), and insulin resistance index (HOMA-IR) in CHOW *versus* GAN groups. (D) Plasma alanine aminotransferase (ALT) and aspartate aminotransferase (AST) levels (U/L), as indicators of liver injury, in CHOW *versus* GAN groups. (E) Effect of Apremilast treatment on body composition. Top left: Δ body weight loss in CHOW and GAN mice treated with vehicle or Apremilast. The remaining graphs show the changes in lean mass and fat mass (grams) from baseline to 2 weeks in each diet group (CHOW or GAN) after Apremilast treatment. (F) Weights (grams) of metabolic tissues (liver, iWAT, eWAT, and mWAT) in CHOW (left) and GAN (right) mice treated with vehicle or Apremilast. (G) Glucose (mg/dL), insulin (μg/L), and HOMA-IR levels in CHOW and GAN mice treated with vehicle or Apremilast. (H) ALT and AST plasma levels (U/L) in CHOW and GAN mice after Apremilast treatment. GAN: Gubra-Amylin NASH diet; CHOW: standard diet; Homeostatic Model Assessment of Insulin Resistance (HOMA-IR); iWAT: inguinal adipose tissue; eWAT: epididymal adipose tissue; mWAT: mesenteric adipose tissue. Data represent mean ± SEM. Statistical significance was assessed using two-way ANOVA, Mann–Whitney *U* test, or Wilcoxon signed-rank test, as appropriate. *P < 0.05.

mass, while lean mass did not differ significantly between groups (Fig. 2B).

At the biochemical level, alterations in serum biomarkers consistent with liver dysfunction and insulin resistance were observed. Elevated insulin levels were also observed, as was the HOMA-IR index, suggesting diet-induced insulin resistance. However, no significant differences were observed in glucose levels (Fig. 2C). In addition, ALT levels were significantly increased in the GAN group, while AST levels showed no statistically significant difference (Fig. 2D).

After two weeks of treatment, apremilast caused a significant reduction in body weight in both groups, although it was more pronounced in animals on the GAN diet compared to mice on the CHOW

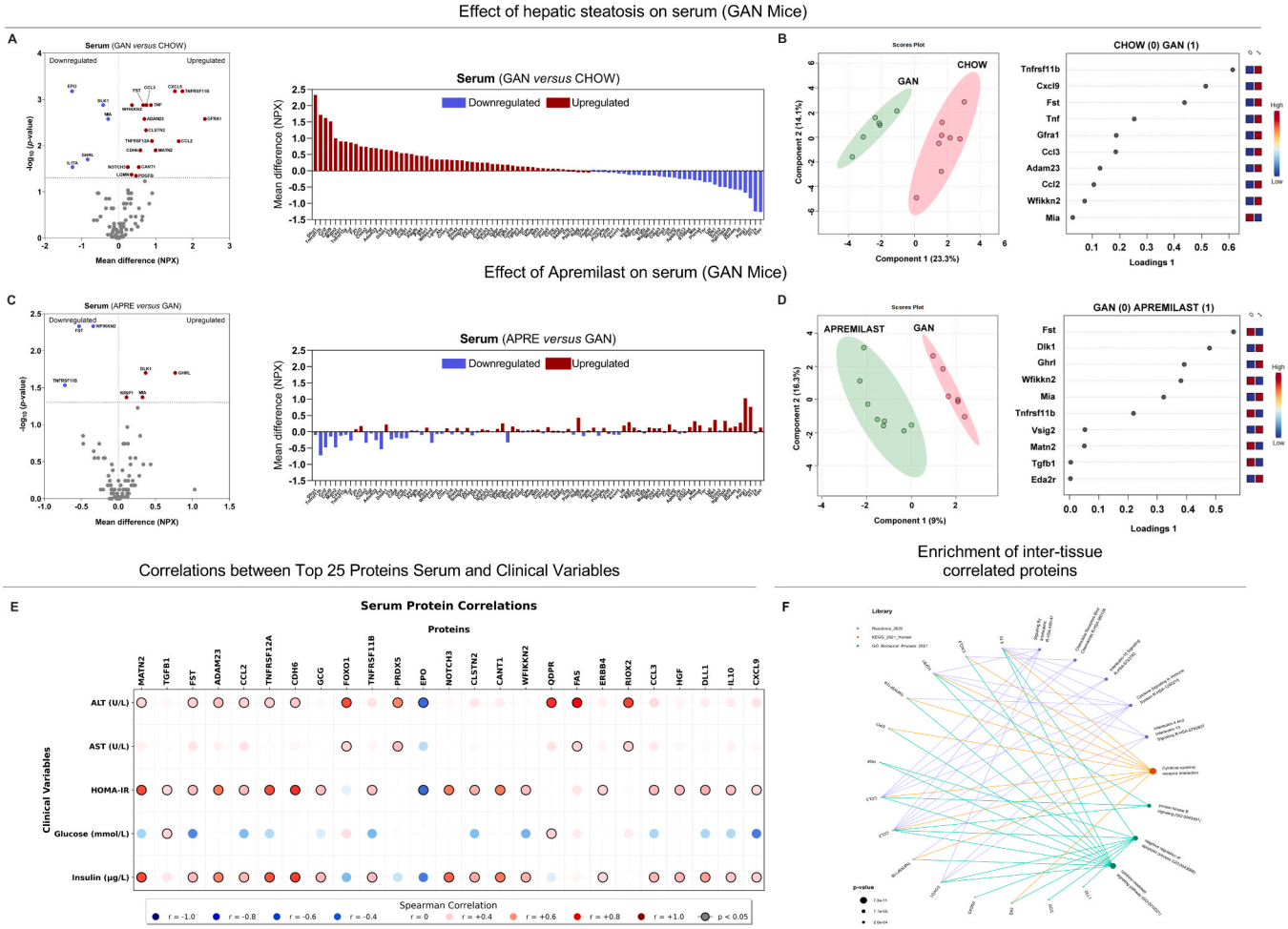

Fig. 3. Serum proteomic profiling in GAN and CHOW mice reveals effects of hepatic steatosis and Apremilast treatment. (A) Volcano plot and fold change analysis of altered proteins from the Olink Target 96 Mouse Exploratory panel comparing GAN *versus* CHOW mice, highlighting significantly upregulated and downregulated proteins. Protein levels are expressed in NPX units (log2-scaled), based on relative quantification. (B) sPLS-DA model discriminates GAN and CHOW mice based on serum proteomic signatures; the corresponding loading plot displays the proteins contributing most to group separation. (C) Volcano plot and fold change of serum proteins comparing Apremilast-treated GAN mice *versus* untreated GAN mice, showing drug-induced proteomic changes. (D) sPLS-DA analysis reveals distinct protein expression patterns between treated and untreated GAN mice, with key discriminatory proteins shown in the loading plot. Statistical analysis was performed using a non-parametric *t*-test (Mann–Whitney *U* test). (E) Bubble plots showing Spearman correlation between the top 25 serum proteins (ranked by variance) and relevant clinical or biochemical variables. The y-axis lists the proteins, and the x-axis the clinical variables. Circle color represents the correlation coefficient (r), ranging from −1 (blue) to + 1 (red), and size indicates significance ($p < 0.05$, black outline). Bolded protein names indicate statistically significant correlations. (F) Enrichment analysis of serum proteints showing strong inter-tissue correlation ($|r| \geq 0.60$), performed using Enrichr. Mouse proteins were mapped to their human orthologs prior to analysis. Enrichment was based on KEGG Human 2021, Reactome 2022, and GO_Biological Process 2021 databases. Significantly enriched pathways are shown, highlighting shared biological processes potentially regulated systemically across metabolic tissues. sPLS-DA: sparse Partial Least Squares Discriminant Analysis; APRE: Apremilast; GAN: Gubra-Amylin NASH diet; CHOW: standard diet. Annotated protein abbreviations are displayed in Supplementary Table 1.

diet. This reduction in GAN mice was associated with a decrease in fat mass, with no changes in lean mass (Fig. 2E), and regression analysis confirmed that the reduction in fat mass was explained by body weight loss (B=0.860, p = 0.009).

A significant decrease in mesenteric adipose tissue weight (mWAT) was also observed, with non-significant trends in epididymal (eWAT) and inguinal adipose tissue (iWAT) (Fig. 2F); this reduction in mWAT was likewise dependent on body weight loss (B=0.089, p = 0.044).

Finally, at the biochemical level, treatment decreased ALT, insulin and HOMA-IR levels without modifications in glucose or AST, suggesting a beneficial effect on liver function and insulin sensitivity in this model (Fig. 2G-H). Regression analyses indicated that the reduction in ALT was independent of body weight loss (B= −160.786, p = 0.055), whereas the decreases in insulin (B=0.466, p = 0.011) and HOMA-IR (B=0.189, p = 0.042) were associated with body weight loss.

Serum Proteomic Changes Associated with Hepatic Steatosis and modulation by PDE4 Inhibition

To dissect the molecular landscape underlying the physiological alterations driven by GAN diet and the effect driven by apremilast, we profiled 92 circulating and tissue-resident proteins. In serum, the induction of steatosis by the GAN diet caused significant alterations in the proteome, reflecting systemic metabolic and inflammatory imbalances. Among the proteins elevated in this context were chemokines and cytokine receptors associated with immune activation and inflammation (CXCL9, CCL2, CCL3, TNFRSF12A, TNF, TNFRSF11B), as well as factors involved in tissue remodeling (MATN2, CDH6, CLSTN2, ADAM23, NOTCH3, CANT1), insulin resistance (FST), fibrogenesis (PDGFB), and cellular stress (LGMN). Conversely, several proteins were downregulated, including EPO, DLK1, MIA, GHRL, and IL17A, suggesting a suppression of repair mechanisms and homeostasis (Fig. 3A). To identify the proteins most strongly associated with the effect of the GAN diet, we applied sparse partial least squares discriminant analysis (sPLS-DA). This multivariate approach revealed a distinct serum proteomic signature that clearly separates steatotic (GAN) from non-steatotic (CHOW) animals. Several of the top discriminating proteins in GAN-fed animals with diet-induced steatosis -such as TNFRSF11B, CXCL9, FST, TNF, GFRA1, ADAM23, CCL2, WFIKKN2, MIA and CCL3- are closely linked to inflammatory pathways, supporting the idea that these animals not only develop steatosis, but also exhibit signs of inflammation, as shown in the loading plot in Fig. 3B.

Apremilast treatment modulated the proteomic profile of mice with GAN diet-induced hepatic steatosis. A reduction in the expression of proteins previously overexpressed in a context of liver dysfunction, such as FST, WFIKK2 and TNFRSF11B, was observed. The reduction in FST suggests a potential improvement in the metabolic, and in insulin sensitivity. While the anti-inflammatory effect of the PDE4 inhibitor itself was observed in the reduction of WFIKK2 and TNFRSF11B levels. An increase in the expression levels of proteins involved in cell differentiation, endocrine signaling and tissue repair (DLK1, GHRL, MIA, WISP1) was also observed (Fig. 3 C). Discriminant analysis of the proteomic data (sPLS-DA) further confirmed a clear separation between untreated and apremilast-treated GAN groups, with FST, DLK1, GHRL, WFIKKN2, MIA, TNFRSF11B, VSIG2, MATN2, TGFB1, and EDA2R emerging as key contributors to group separation (Fig. 3D). In contrast, in standard diet (CHOW) animals treated with PDE4 inhibitor, serum changes were minimal, reducing the levels of cell adhesion-related proteins (PLXNA4, ADAM23) (Supplemental figure 1A).

Fig. 3E shows a correlation bubble plot illustrating the 25 proteins most strongly associated with clinical and metabolic parameters modulated by the GAN diet and apremilast treatment. Data from all experimental groups (Chow, GAN, Chow+Apremilast, GAN+Apremilast) were pooled to cover the full spectrum from disease to pharmacological reversal. Strong correlations ($|r| > 0.6$; $p < 0.01$) emerged between several proteins and key indicators of liver damage and metabolic dysfunction. Several proteins demonstrated strong and significant correlations with key metabolic parameters, including ALT, AST, HOMA-IR, and insulin. Notably, insulin and HOMA-IR levels strongly correlated with serum proteins such as MATN2, ADAM23, CCL2, TNFRF12A, CDH6, TNFRF12B, NOTCH3, CLSTN2, CANT1, CCL3, HGF, DLL1, IL10 and CXCL9, among others. Both AST and ALT levels correlated with FOXO1, PRDX5, FAS and RIOX2. Besides, ALT strongly correlated with MATN2, TGFB1, ADAM23, CCL2, TNFRF12A, CDH6 and QDPR. These findings indicate coordinated variation between circulating protein levels and metabolic and liver indicators (Fig. 3E). To gain insight into the biological significance of proteins most strongly correlated with clinical parameters, we performed a functional enrichment analysis. Mouse protein identifiers were first mapped to their human orthologs, and subsequent enrichment was carried out using Gene Ontology (GO) Biological Process, KEGG Human pathways, and Reactome databases.

This analysis revealed a significant overrepresentation of immune- and inflammation-related pathways, including signaling by interleukins, chemokine receptors bind chemokines, Interleukin-10 signaling, cytokine signaling in the immune system, Interleukin-4 and Interleukin-13 signaling, and Cytokine–cytokine receptor interaction. Additional enriched categories involved protein kinase B signaling and negative regulation of apoptotic processes, as well as the broader cytokine-mediated signaling pathway. Many of these pathways have established roles in leukocyte recruitment, modulation of inflammatory tone, and regulation of hepatocyte survival, supporting their contribution to the alterations in body weight, insulin resistance, and liver injury observed in GAN-fed animals, and highlighting potential mechanisms through which apremilast may exert its effects (Fig. 3F).

3.3. Liver fibrosis and steatosis are attenuated by apremilast treatment

To evaluate the histopathological impact of the GAN diet and the therapeutic effects of apremilast, immunohistochemical analyses of liver tissue were conducted. As shown in Fig. 4A, GAN-fed mice exhibited a significantly higher percentage of hepatic fibrosis compared to control animals, confirming the fibrogenic effects of prolonged metabolic stress. Remarkably, treatment with apremilast effectively reversed fibrosis, leading to a significant reduction in the fibrotic area. A comparable, although less pronounced, reduction in fibrosis was also observed in CHOW-fed mice treated with apremilast, suggesting a basal antifibrotic effect of the PDE4 inhibitor even in the absence of dietary-induced liver damage.

In parallel, the evaluation of hepatic lipid accumulation (Fig. 4B) revealed a marked increase in intracellular lipid droplets in GAN-fed mice vs control group, consistent with severe steatosis. Apremilast treatment showed a trend toward reduced lipid droplet accumulation in both GAN and CHOW groups, although this did not reach statistical significance, suggesting a potential role of PDE4 inhibition in improving hepatocellular lipid handling.

Together, these histological findings support a dual action of apremilast in the liver, mitigating fibrotic remodeling and potentially alleviating steatotic burden, under pathological and basal conditions.

3.4. Comprehensive proteomic profiling of the liver in GAN diet and apremilast-treated mice

Hepatic proteomic analyses in GAN mice revealed a marked proinflammatory environment, with alterations in inflammation-associated proteins (IL1A, CCL2, CCL3, CCL5, CCL20), apoptotic pathways (FOXO1, CASP3, TNFSF12, MAP2K6), cell adhesion and migration (APBB1IP, S100A4, ADAM23), lipid metabolism (PLA2G4A), cell signaling (AXIN1, TGFBR3, ERBB4), intracellular transport (DCTN2) and oxidative stress (PRDX5, QDPR) (Fig. 5**A**). Taken together, these changes suggest a widespread dysregulation of inflammation, cell death and liver repair mechanisms.

Fig. 5B displays the results of a sPLS-DA comparing the GAN vs. CHOW. This multivariate approach highlights the proteins that best

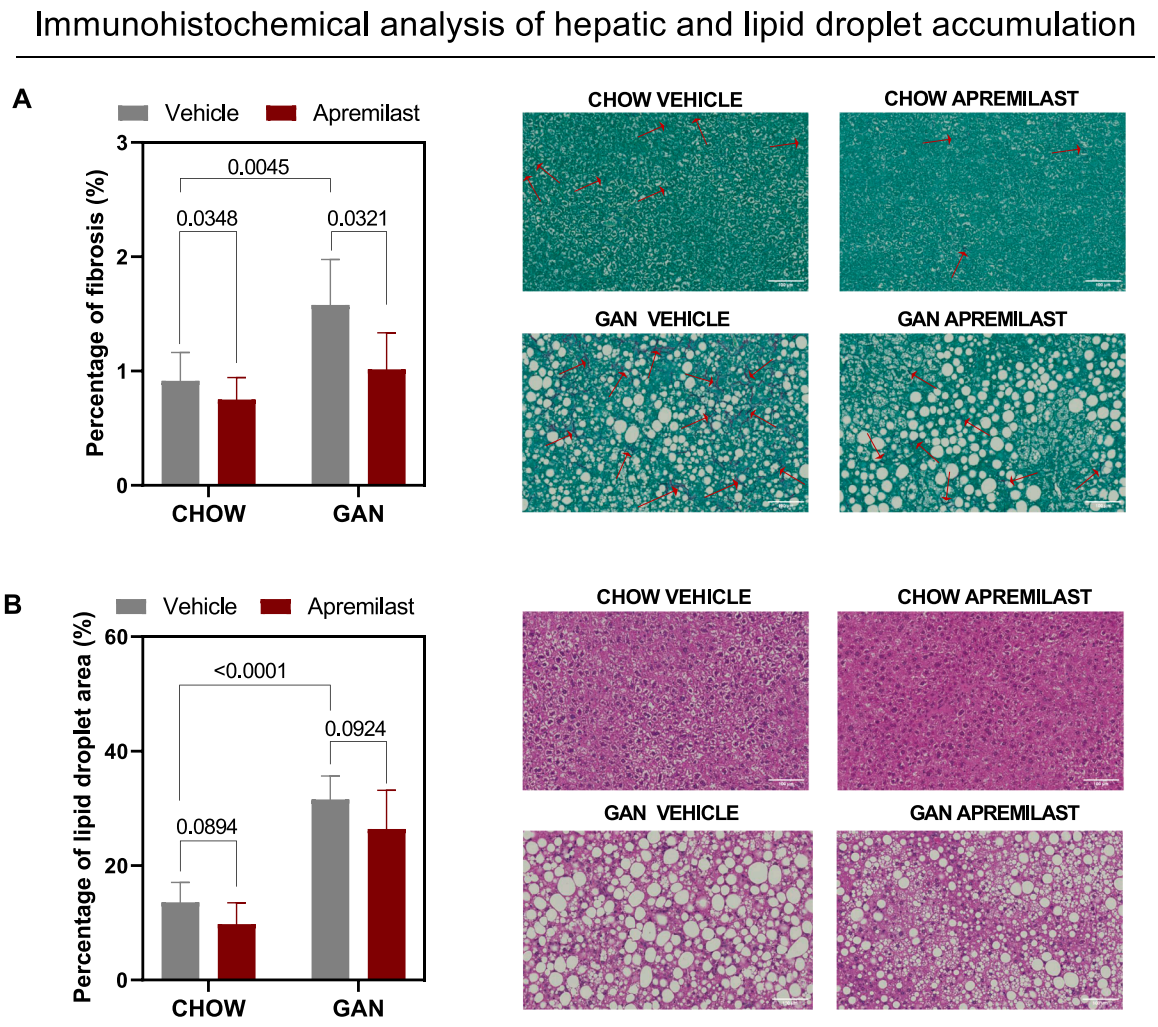

Fig. 4. Histological analysis of liver fibrosis and steatosis in GAN and CHOW mice treated with Apremilast. (A) Quantification and representative images of hepatic fibrosis. The percentage of fibrotic area was quantified using ImageJ software from Picro-Sirius Red (PSR) staining. Representative liver sections from CHOW and GAN mice treated with vehicle or Apremilast are shown (scale bar = 100 μm). Red staining indicates collagen fibers; arrows highlight fibrotic regions. (B) Quantification and representative images of hepatic steatosis. The percentage of lipid droplet area was measured in H&E-stained liver sections (scale bar = 100 μm) from CHOW and GAN mice treated with vehicle or Apremilast. Representative images illustrate the degree of lipid accumulation across groups. Quantitative histomorphometric assessment of liver lipid accumulation (H&E staining) and fibrosis (PSR staining) was performed. *P < 0.05 vs. corresponding control group, 2-way ANOVA test. GAN: Gubra-Amylin NASH diet; CHOW: standard diet.

discriminate between GAN and CHOW liver profiles, which, in addition to the presence or absence of steatosis, also differ in their levels of inflammation and fibrosis. Key discriminative proteins include CCL2, TNFRSF12A, WFIKKN2, TNF, AXIN1, ADAM23, S100A4, and FST. These proteins form a distinct hepatic signature of GAN-induced steatosis, reinforcing their relevance as potential biomarkers of liver dysfunction.

Apremilast treatment significantly modulated the liver proteome, promoting the expression of proteins with anti-fibrotic functions and reducing the presence of those associated with apoptosis, oxidative stress and metabolic dysfunction (Fig. 5**C**). Although not all changes reached statistical significance, the fold change analysis in Fig. 5C (right panel) reveals that apremilast induced broad proteomic remodeling in the liver, affecting the expression of nearly all proteins measured. The significantly regulated proteins included PARP1, DCTN2, LGMN, DDAH1, FOXO1, QDPR, CASP3, NADK, WFIKKN2 and FSTL3. A distinctive protein signature composed of VSIG2, LPL, EDA2R, AHR, AHR, IL23R, IGSF3, LGMN, PDGFB, CYR61 and GFRA1 was also identified and clearly differentiated the treated groups (Fig. 5D). In contrast, in standard diet animals treated with the PDE4 inhibitor, hepatic changes were minimal, with a reduction observed in the level of a single protein, SEZ6L2 (Supplementary figure 1B).

3.5. Proteomic remodeling of visceral adipose tissue in response to GAN diet and apremilast treatment

After steatosis induction, proteomic analysis showed significant changes in the expression of multiple proteins in visceral adipose tissue. In eWAT, increased expression of several proteins involved in inflammatory processes, extracellular matrix remodeling, and cell signaling was observed. Notable upregulated proteins include S100A4, CYR61, AXIN1, CXCL9, PDGFB, CASP3, CCL3, AHR, HGF, APBB1IP, RIOX2, CCL5, CCL2, PLA2G4A, SNAP29, KITLG, EDA2R, PARP1, TNFSF12, WISP1, DDAH1, FST, and MATN2 (Fig. 6A). Fig. 6B presents the corresponding sPLS-DA analysis, highlighting proteins that best discriminate eWAT GAN from CHOW animals. The top discriminative features include S100A4, CASP3, APBB1IP, AXIN1, CYR61, CCL3, AHR, RIOX2, HGF, and CCL2, forming a distinct proteomic signature reflective of adipose tissue inflammation and dysfunction in response to GAN diet.

Apremilast treatment in GAN mice modulated the proteome of visceral adipose tissue. Although not all changes reached statistical significance, the fold change analysis in Fig. 6C (right panel) reveals that apremilast induced broad proteomic remodeling in the eWAT, affecting the expression of nearly all proteins measured. Apremilast significantly

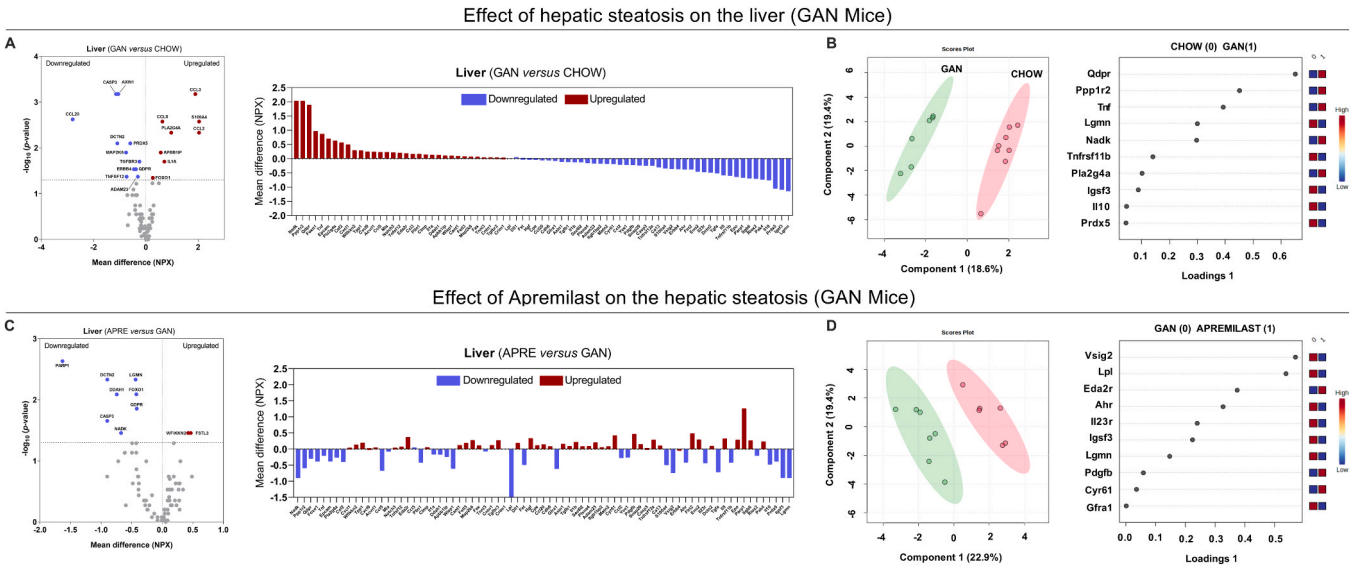

Fig. 5. Liver proteomic in GAN and CHOW mice reveals the impact of hepatic steatosis and Apremilast treatment. (A) Volcano plot and fold change analysis of altered proteins from the Olink Target 96 Mouse Exploratory panel comparing GAN *versus* CHOW mice, highlighting significantly upregulated and downregulated proteins. Protein levels are expressed in NPX units (log2-scaled), based on relative quantification. (B) sPLS-DA model discriminates GAN and CHOW mice based on serum proteomic signatures; the corresponding loading plot displays the proteins contributing most to group separation. (C) Volcano plot and fold change of serum proteins comparing Apremilast-treated GAN mice *versus* untreated GAN mice, showing drug-induced proteomic changes. (D) sPLS-DA analysis reveals distinct protein expression patterns between treated and untreated GAN mice, with key discriminatory proteins shown in the loading plot. Statistical analysis was performed using a non-parametric *t*-test (Mann–Whitney *U* test). sPLS-DA: sparse Partial Least Squares Discriminant Analysis; APRE: Apremilast; GAN: Gubra-Amylin NASH diet; CHOW: standard diet. Annotated protein abbreviations are displayed Supplementary Table 1.

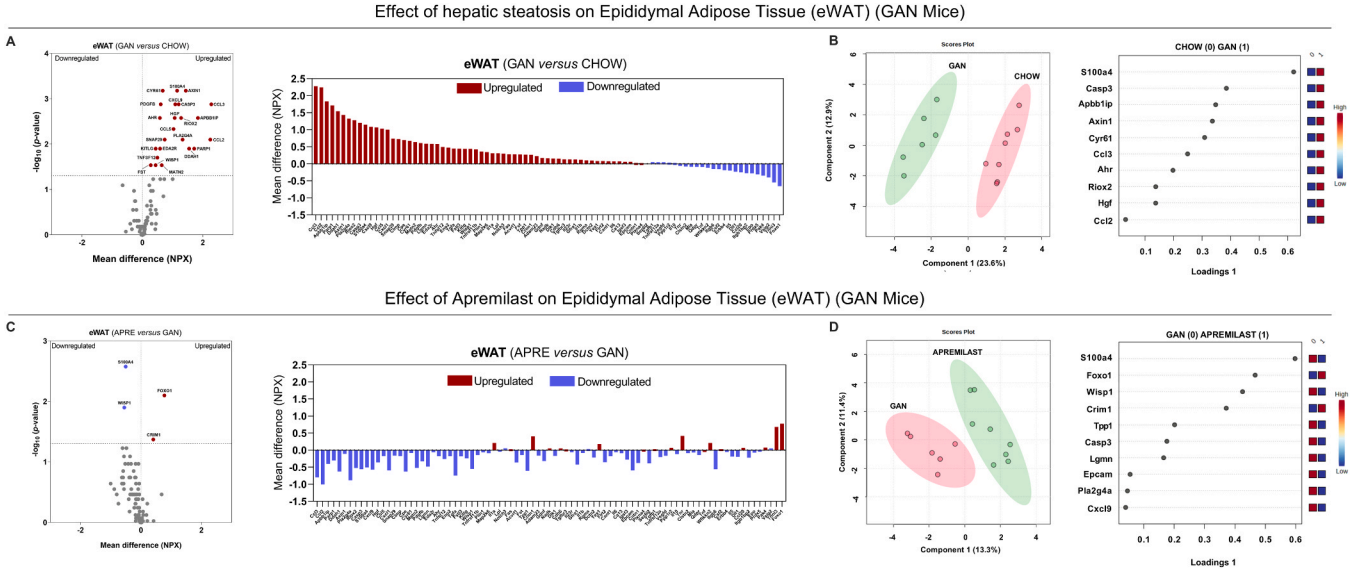

Fig. 6. Effects of GAN diet and Apremilast treatment in eWAT proteomic profile (A) Volcano plot and fold change analysis of altered proteins from the Olink Target 96 Mouse Exploratory panel comparing GAN *versus* CHOW mice, highlighting significantly upregulated and downregulated proteins. Protein levels are expressed in NPX units (log2-scaled), based on relative quantification. (B) sPLS-DA model discriminates GAN and CHOW mice based on serum proteomic signatures; the corresponding loading plot displays the proteins contributing most to group separation. (C) Volcano plot and fold change of serum proteins comparing Apremilast-treated GAN mice *versus* untreated GAN mice, showing drug-induced proteomic changes. (D) sPLS-DA analysis reveals distinct protein expression patterns between treated and untreated GAN mice, with key discriminatory proteins shown in the loading plot. Statistical analysis was performed using a non-parametric *t*-test (Mann–Whitney *U* test). sPLS-DA: sparse Partial Least Squares Discriminant Analysis; APRE: Apremilast; GAN: Gubra-Amylin NASH diet; CHOW: standard diet; eWAT: epididymal adipose tissue. Annotated protein abbreviations are displayed Supplementary Table 1.

reduced the expression of pro-inflammatory proteins such as S100A4 and WISP1, while increasing the levels of FOXO1 and CRIM1 (Fig. 6**C**). Fig. 6D shows the sPLS-DA analysis, which identifies a robust separation between the treated and untreated GAN groups. Discriminative proteins include CCL3, PDGFB, SNAP29, S100A4, FST, and CRIM1, consistent with the anti-inflammatory and metabolic effects of apremilast on eWAT.

In CHOW mice treated with apremilast, a reduction in the expression of several proteins was observed in eWAT (Supplementary figure 1C). Specifically, apremilast lowered the levels of seven proteins -MAP2K6, PAK4, NADK, FOXO1, EPCAM, WISP1, and CLSTN2- which have been implicated in diverse cellular processes, including signaling,

metabolism, and tissue organization.

3.6. Skeletal muscle proteomic alterations induced by steatosis are discreted modulated by PDE4 inhibition

Analysis of the muscle proteome in mice with induced hepatic steatosis revealed significant alterations in nine proteins including increased levels of MAP2K6, MATN2, GFRA1, PLIN1, PARP1, FAS, CLMP and ACVRL1 and reduced levels of PPP1R2, many of which are linked to lipid metabolism, fibrosis, and stress signaling (Fig. 7A). In addition, a protein signature composed of ten proteins was identified that allowed a clear distinction between the GAN and control groups (MAP2K6, PPP1R2, PLIN1, GFRA1, PARP1, MATN2, FAS, ACVRL1, CNTN1 and YES1) (Fig. 7B).

Treatment with the PDE4 inhibitor in GAN mice partially modulated steatosis-induced protein alterations, particularly by reducing significantly previously elevated proteins such as MAP2K6 and PLIN1, as well as ENO2 and CCL2 (Fig. 7C). Although many changes did not reach statistical significance, the fold change analysis in Fig. 7C (right panel) indicates that apremilast induces widespread remodeling of the skeletal muscle proteome, altering the expression levels of all many proteins assessed. Analysis by sPLS-DA identified a differential protein profile associated with apremilast treatment in skeletal muscle, consisting of the following proteins: PLIN1, MAP2K6, ENO2, CCL2, RGMA, TGFA, CNTN1, PRDX5, LPL and DDAH1 (Fig. 7D).

In CHOW mice, treatment with apremilast induced an overexpression of PDGFB, a factor linked to angiogenesis and tissue remodeling, and a decrease in DDAH1 levels, which may reduce nitric oxide signaling, suggesting vascular remodeling that could impact muscle metabolism (Supplementary figure 1D).

3.7. Shared and distinct proteomic fingerprints emerge across tissues following GAN-induced steatosis

The GAN diet induced a tissue-specific proteomic response, with each organ displaying a distinct set of significantly altered proteins: liver, eWAT, skeletal muscle, and serum. When considering the total number of unique proteins altered across compartments, the most affected tissues were serum and eWAT, followed by the liver and skeletal muscle (Supplementary Figure 2A).

While most proteomic changes were specific to individual tissues, a subset of proteins exhibited consistent alterations across multiple compartments. In particular, MATN2, CCL2, and CCL3 were dysregulated in at least three tissues, pointing to a shared inflammatory and tissue remodeling signature induced by the GAN diet. Notably, the greatest overlap of altered proteins occurred between the liver and eWAT (Supplementary Figure 2B).

3.8. Tissue-specific proteomic modulation by apremilast in GAN mice

Apremilast induced a selective and tissue-specific modulation of protein expression, with minimal overlap between compartments. In total, 22 proteins were significantly altered in at least one tissue. Among these, only three proteins—WFIKKN2, WISP1, and FOXO1—were modulated in more than one compartment, suggesting limited systemic convergence and emphasizing the organ-specific action of PDE4 inhibition (Supplementary Figure 3A).

The liver remained one of the most affected organs, showing significant downregulation of proteins associated with apoptosis, oxidative stress, and metabolic dysfunction (e.g., CASP3, LGMN, DDAH1, PARP1), in line with the observed histological and clinical improvements. In eWAT, apremilast significantly modulated inflammation- and remodeling-related proteins, including S100A4, WISP1, and CRIM1, while in skeletal muscle, proteins such as CCL2, PLIN1, and MAP2K6 were downregulated, pointing to an attenuation of stress and lipid metabolism pathways. In the serum, reduced levels of FST, TNFRSF11B, and WFIKKN2 further reflect the systemic anti-inflammatory and metabolic effects of treatment (Supplementary Figure 3B).

4. Discussion

Our study provides evidence that apremilast reduce liver enzyme

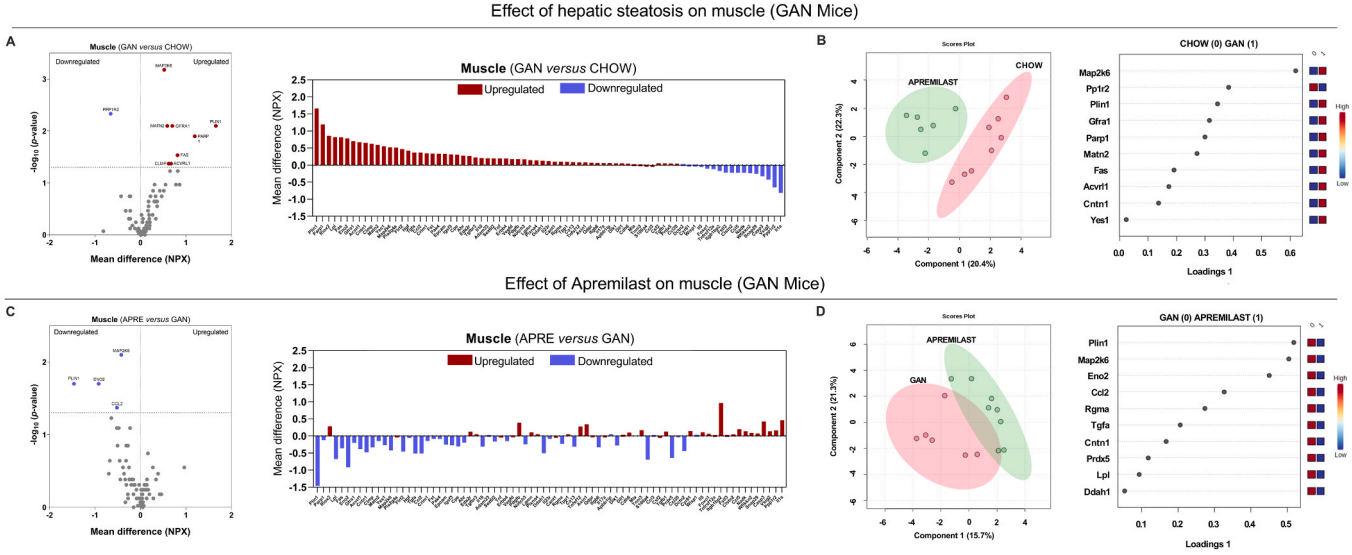

Fig. 7. Effects of GAN diet and Apremilast treatment in skeletal muscle proteomic profile (A) Volcano plot and fold change analysis of altered proteins from the Olink Target 96 Mouse Exploratory panel comparing GAN *versus* CHOW mice, highlighting significantly upregulated and downregulated proteins. Protein levels are expressed in NPX units (log2-scaled), based on relative quantification. (B) sPLS-DA model discriminates GAN and CHOW mice based on serum proteomic signatures; the corresponding loading plot displays the proteins contributing most to group separation. (C) Volcano plot and fold change of serum proteins comparing Apremilast-treated GAN mice *versus* untreated GAN mice, showing drug-induced proteomic changes. (D) sPLS-DA analysis reveals distinct protein expression patterns between treated and untreated GAN mice, with key discriminatory proteins shown in the loading plot. Statistical analysis was performed using a non-parametric *t*-test (Mann–Whitney *U* test). sPLS-DA: sparse Partial Least Squares Discriminant Analysis; APRE: Apremilast; GAN: Gubra-Amylin NASH diet; CHOW: standard diet. Annotated protein abbreviations are displayed Supplementary Table 1.

levels and the hepatic steatosis index in real-world cohort of patients with psoriatic arthritis and metabolic comorbidities. In parallel, we demonstrate in a murine model of MASLD that apremilast reduces hepatic steatosis and fibrosis, accompanied by significant improvements in body weight, insulin resistance, and circulating liver enzymes.

At the molecular level, this is the first study to comprehensively characterize the proteomic alterations across key metabolic tissues—including liver, visceral adipose tissue, skeletal muscle, and serum—in response to the GAN diet. Notably, apremilast modulated protein expression in a tissue-specific manner, with the most profound effects observed in the liver. Collectively, these findings not only highlight the systemic and compartmentalized impact of PDE4 inhibition, but also open new avenues for personalized therapeutic strategies in patients with NAFLD/MASLD, particularly those with coexisting psoriatic disease, where inflammation and metabolic dysregulation intersect.

We first examined a real-world cohort of patients with PsA, a population commonly affected by metabolic comorbidities such as obesity, insulin resistance, and NAFLD [17]. By applying a stratification approach based on the presence of metabolic alterations, we identified a subgroup of patients who not only exhibited clinical features consistent with systemic metabolic dysfunction, but also responded to apremilast treatment with improvements in hepatic and glycemic parameters. Specifically, patients in the metabolically compromised cluster showed reductions in fasting insulin, HOMA-IR, transaminases (ALT and AST), and the HSI after 6 months of treatment. These observations suggest that apremilast may exert systemic immunometabolic effects other than joint and skin inflammation, supporting the concept that PDE4 inhibition could also confer metabolic and hepatoprotective benefits against MASLD.

To explore this hypothesis mechanistically, we used the GAN diet model to promote MASLD, which recapitulates key features of the human condition, including obesity and hepatic steatosis [18]. As expected, mice fed the GAN diet developed a metabolically compromised phenotype, including weight gain, increased adiposity, and insulin resistance, as reflected by elevated insulin levels and HOMA-IR scores. This preclinical model provided a relevant pathophysiological model to evaluate the therapeutic effects of apremilast.

To date, there is little information regarding the role of PDE4 inhibitors in liver disease. The only published study exploring this class of compounds in vivo in the context of MASLD is the recent work *by Wang et al.*, which demonstrated that roflumilast ameliorates hepatic steatosis and fibrosis in ob/ob mice fed the GAN diet by targeting hepatic lipid accumulation, inflammation, and fibrogenesis [19]. While these findings support the therapeutic relevance of PDE4 inhibition in MASLD, no studies have yet investigated the effects of apremilast—the only approved PDE4 inhibitor for the treatment of PsA—in this setting. Here, we provide the first evidence of the metabolic and hepatoprotective actions of apremilast in the context of GAN diet-induced MASLD.

Treatment with apremilast resulted in marked metabolic improvements in mice fed the GAN diet. Notably, apremilast led to a reduction in body weight specifically in GAN-fed animals, which was primarily driven by a decrease in fat mass, while lean mass remained unchanged. At the metabolic level, apremilast lowered circulating insulin levels and improved insulin sensitivity, as reflected by a reduction in HOMA-IR, without altering glucose concentrations. These findings indicate an enhancement of systemic insulin responsiveness, likely linked to the reduction in adipose tissue inflammation and ectopic fat deposition. Furthermore, a significant decrease in ALT levels was observed in GAN-fed mice treated with apremilast, suggesting a potential hepatoprotective effect, although AST levels remained unchanged. Collectively, these data support the beneficial metabolic actions of apremilast in a context of diet-induced hepatic steatosis, reinforcing its potential utility in the management of MASLD.

The metabolic improvements observed with apremilast in murine models—such as weight loss, reduced inflammation, and improved insulin sensitivity—are consistent with clinical trial data showing its ability to lower body weight, increase HDL, reduce LDL and HbA1c levels [11], and decrease cardiovascular risk markers [12]. These findings highlight the dual anti-inflammatory and metabolic benefits of apremilast in both experimental and clinical settings.

At hepatic tissue level, apremilast significantly reduced fibrosis and showed a trend toward reducing steatosis**,** as demonstrated by immunohistochemical analysis. Notably, the significant antifibrotic effect together with the tendency to lower hepatocellular lipid accumulation supports the idea that apremilast not only modulates systemic metabolic parameters but also exerts local effects on liver metabolism, mitigating key hallmarks of MASLD progression.

Our integrated proteomic analysis provides the first comprehensive characterization of the tissue-specific molecular alterations induced by the GAN diet across key metabolic organs, including the liver, visceral adipose tissue, skeletal muscle, and serum. Hepatic steatosis was associated with a broad and compartmentalized systemic response, involving not only local hepatic changes but also proteomic remodeling in peripheral tissues. The majority of proteomic changes induced by the GAN diet were tissue-specific. However, our analysis identified a subset of proteins (MATN2, CCL2, and CCL3) that were consistently dysregulated across multiple compartments. These proteins are closely linked to extracellular matrix remodeling, monocyte recruitment, and inflammatory activation [20–22], suggesting that the diet triggers a marked systemic immunometabolic signature. Notably, the strongest overlap of proteomic alterations was observed between the liver and visceral adipose tissue (eWAT)—two metabolically active organs that are tightly interrelated in obesity-associated pathologies. This overlap supports the notion of a bidirectional communication axis between liver and adipose tissue, where inflammatory and fibrotic signaling cascades in one compartment may influence or exacerbate dysfunction in the other. Such crosstalk is consistent with clinical observations linking visceral adiposity to hepatic steatosis and fibrosis, and highlights the importance of targeting both organs to effectively modulate the immunometabolic burden in MASLD [23].

Importantly, treatment with apremilast reversed some of these pathological signatures, especially in the liver, where it downregulated a number of inflammatory and fibrogenic mediators while enhancing proteins involved in tissue repair and metabolic balance (FOXO1, WFIKKN2, DCTN2, QDPR, PARP1, NADK, DDAH1, LGMN, CASP3 and FSTL3) [24,25]. This study also highlights the tissue-specific nature of apremilast's action: while each organ responded with a unique proteomic alteration. Among the 28 altered proteins, four (WISP1, WFIKKN2, FOXO1, and MAP2K6) were shared across multiple tissues or serum. WISP1 is a novel adipokine secreted by mature adipocytes, whose expression is elevated in both visceral and subcutaneous adipose tissue in the context of obesity. It has been shown to correlate with systemic inflammation and insulin resistance, promoting the production of proinflammatory cytokines and potentially contributing to macrophage polarization within adipose tissue. Moreover, WISP1 has also been implicated in hepatic inflammation and may play a role in the pathogenesis of NAFLD [26]. Another common altered protein, WFIKKN2, is a circulating protease inhibitor that modulates members of the TGF-β family. Recent proteomic studies have identified it as a promising biomarker in metabolic disease, with elevated levels associated with improved glycaemic control and reduced risk of DM2, possibly through its role in energy homeostasis via cell signaling pathways [27]. In the liver, FOXO1 acts as a key transcriptional regulator involved in lipid metabolism, inflammation, and the cellular stress response. Its persistent activation has been linked to insulin resistance, hepatic steatosis, and progression to NASH [28], and it also plays a role in endothelial metabolic regulation and vascular homeostasis [29]. MAP2K6, a kinase within the p38 MAPK signaling cascade, has also emerged as a relevant modulator of hepatic lipid metabolism. Overexpression of MAP2K6 in murine models resulted in reduced hepatic triglyceride content and improved metabolic parameters, including plasma glucose, insulin, and adiposity, suggesting a protective role in diet-induced metabolic

dysfunction [30]. Taken together, these findings support a compartmentalized therapeutic response to apremilast, with distinct and common molecular pathways targeted in each tissue. This underscores the value of a multi-tissue proteomic approach to capture the full therapeutic landscape of PDE4 inhibition in MASLD.

5. Conclusions

In summary, this study provides the first comprehensive evaluation of the anti-inflammatory signature of apremilast in the context of diet-induced steatotic liver disease. In a real-world clinical cohort of patients with psoriatic arthritis, apremilast significantly improved glycemic and hepatic markers in those with coexisting metabolic comorbidities. By using a dietary murine model of MASLD, we further demonstrate that apremilast improves key clinical features of metabolic dysfunction, including reductions in fat mass, insulin resistance, and liver enzyme levels. Histological analyses confirmed its ability to reduce fibrosis, highlighting a direct protective effect on liver. At the molecular level, we present the first multi-tissue proteomic atlas of GAN-induced steatosis, revealing both tissue-specific and systemic protein alterations across liver, visceral adipose tissue, skeletal muscle, and serum. Apremilast modulated these pathological signatures in a compartmentalized manner, reversing inflammation- and fibrosis-related pathways while promoting markers of tissue repair and metabolic homeostasis, thereby validating the translational relevance of our findings. Together, these results support a novel role for PDE4 inhibition in the management of MASLD associated to PSD and underscore the potential of apremilast as a personalized immunometabolic therapy in patients with psoriatic disease having an altered metabolic profile.

One limitation of our study is that the preclinical experiments were conducted exclusively in male mice, which may limit the generalizability of the findings to females. This decision was based on feasibility, the limited amount of apremilast, and the need to avoid hormonal variability linked to estrogens, which are known to protect against hepatic steatosis and insulin resistance. However, future studies should include both sexes to explore potential sex-specific responses.

CRediT authorship contribution statement

Pedro Ortiz-Buitrago: Writing – review & editing, Methodology. **Alejandro Escudero-Contreras:** Writing – review & editing, Resources. **Jesús Eduardo Martín-Salazar:** Writing – review & editing, Methodology, Data curation. **Chary Lopez-Pedrera:** Writing – review & editing, Resources. **Sergio Rodríguez-Cuenca:** Writing – review & editing, Validation, Supervision, Project administration, Methodology, Investigation, Data curation, Conceptualization. **ClementinaLópez-Medina:** Writing – review & editing, Resources. **Carlos Perez-Sanchez:** Writing – review & editing, Methodology. **Iván Arias-de la Rosa:** Writing – review & editing, Writing – original draft, Visualization, Validation, Supervision, Methodology, Formal analysis, Conceptualization. **Mark Campbell:** Writing – review & editing, Supervision, Methodology, Investigation, Conceptualization. **Antonio Vidal-Puig:** Writing – review & editing, Supervision, Project administration, Investigation, Funding acquisition, Conceptualization. **Adrian Llamas-Urbano:** Writing – review & editing, Methodology. **Maria Dolores Lopez-Montilla:** Writing – review & editing, Resources, Data curation. **Barbarroja Puerto Nuria:** Writing – review & editing, Supervision, Project administration, Funding acquisition, Conceptualization. **Laura Romero-Zurita:** Writing – review & editing, Visualization, Formal analysis. **Antonio Manuel Barranco:** Writing – review & editing, Methodology. **Laura Cuesta-López:** Writing – review & editing, Methodology. **Miriam Ruiz-Ponce:** Writing – review & editing, Writing – original draft, Visualization, Validation, Methodology, Investigation, Formal analysis, Data curation, Conceptualization. **Eduardo Collantes-Estevez:** Writing – review & editing, Resources. **Julio M. Martínez-Moreno:** Writing – review & editing, Methodology.

Funding

This work was supported by grants from the Minister of Science, Innovation and Universities (PID2022–141500OA-I00, PID2023–152503OB-I00). C.P-S was supported by contracts from MINECO (RYC2021–033828-I) cofounded by the European Union NextGenerationEU/PRTR. LCL was supported by contracts from Minister of Science, Innovation and Universities (FPU20/06329). MRP and JEMS were supported by contracts from Instituto de Salud Carlos III (FI21/00039 and FI23/00233, respectively).

SRC, MC and TVP were funded by the Medical Research Council (MC_UU_00039/2); and the Wellcome Trust [grant number 226800/Z/22/Z]. The IMS-MRL Histopathology Core and the Disease Model Cores were funded by the Medical Research Council (MC_MC_ UU_00039), and Wellcome Trust [grant number 226800/Z/22/Z]. MRC MDU Mouse Biochemistry Laboratory was supported by the Medical Research Council (MC_UU_00014/5), and the NIHR Biomedical Research Centre (NIHR203312). The views expressed are those of the authors and not necessarily those of the NIHR or the Department of Health and Social Care.

Declaration of Competing Interest

The authors declare that there are no conflicts of interest. C.P-S and N.B are co-founders of Cobiomic Bioscience S.L.

Acknowledgments

This work included studies performed under the Amgen Research Agreement No: 5098797, involving the evaluation of Apremilast.

"We would like to acknowledge staff at the IMS-MRL Disease Model Core for in vivo metabolic phenotyping and the Histology Core and MRC MDU Mouse Biochemistry Laboratory for the processing of the histological and biochemistry samples respectively."

Appendix A. Supporting information

Supplementary data associated with this article can be found in the online version at doi:10.1016/j.biopha.2025.118757.

Data availability

Data will be made available on request.

References

[1] Y.S. Chiu, C.C. Wei, Y.J. Lin, Y.H. Hsu, M.S. Chang, IL-20 and IL-20R1 antibodies protect against liver fibrosis, Hepatology 60 (3) (2014) 1003–1014, https://doi.org/10.1002/hep.27189.

[2] C. Estes, Q.M. Anstee, M.T. Arias-Loste, H. Bantel, S. Bellentani, J. Caballeria, M. Colombo, A. Craxi, J. Crespo, C.P. Day, Y. Eguchi, A. Geier, L.A. Kondili, D. C. Kroy, J.V. Lazarus, R. Loomba, M.P. Manns, G. Marchesini, A. Nakajima, H. Razavi, Modeling NAFLD disease burden in China, France, Germany, Italy, Japan, Spain, United Kingdom, and United States for the period 2016–2030, J. Hepatol. 69 (4) (2018) 896–904, https://doi.org/10.1016/j.jhep.2018.05.036.

[3] V.W. Wong, M. Ekstedt, G.L. Wong, H. Hagström, Changing epidemiology, global trends and implications for outcomes of NAFLD, J. Hepatol. 79 (3) (2023) 842–852, https://doi.org/10.1016/j.jhep.2023.04.036.

[4] European Association for the Study of the Liver (EASL), European Association for the Study of Diabetes (EASD), & European Association for the Study of Obesity (EASO). (2024). EASL-EASD-EASO clinical practice guidelines on the management of metabolic dysfunction-associated steatotic liver disease (MASLD). Journal of Hepatology, 81(3), 492–542. https://doi.org/10.1016/j.jhep.2024.04.031.

[5] N. Stefan, H.U. Häring, K. Cusi, Non-alcoholic fatty liver disease: causes, diagnosis, cardiometabolic consequences, and treatment strategies, Lancet Diabetes Endocrinol. 7 (4) (2019) 313–324, https://doi.org/10.1016/S2213-8587(18)30154-2.

[6] A. Ortolan, M. Lorenzin, G. Tadiotto, F.P. Russo, F. Oliviero, M. Felicetti, R. D'Incà, M. Favero, S. Piaserico, A. Doria, R. Ramonda, Metabolic syndrome, non-alcoholic fatty liver disease and liver stiffness in psoriatic arthritis and psoriasis patients, Clin. Rheumatol. 38 (10) (2019) 2843–2850, https://doi.org/10.1007/s10067-019-04646-7.

[7] N. Barbarroja, M. Ruiz-Ponce, L. Cuesta-López, C. Pérez-Sánchez, C. López-Pedrera, I. Arias-de la Rosa, E. Collantes-Estévez, Nonalcoholic fatty liver disease in inflammatory arthritis: Relationship with cardiovascular risk, Front. Immunol. 13 (2022) 997270, https://doi.org/10.3389/fimmu.2022.997270.
[8] Z. Ruan, T. Lu, Y. Chen, M. Yuan, H. Yu, R. Liu, X. Xie, Association between psoriasis and nonalcoholic fatty liver disease among outpatient US adults, JAMA Dermatol. 158 (7) (2022) 745–753, https://doi.org/10.1001/jamadermatol.2022.1609.
[9] R. Candia, A. Ruiz, R. Torres-Robles, N. Chávez-Tapia, N. Méndez-Sánchez, M. Arrese, Risk of non-alcoholic fatty liver disease in patients with psoriasis: a systematic review and meta-analysis, J. Eur. Acad. Dermatol. Venereol. 29 (4) (2015) 656–662, https://doi.org/10.1111/jdv.12847.
[10] M. Ruiz-Ponce, L. Cuesta-López, M.D. López-Montilla, C. Pérez-Sánchez, P. Ortiz-Buitrago, A. Barranco, M.D. Gahete, N. Herman-Sánchez, A.J. Lucendo, P. Navarro, C. López-Pedrera, A. Escudero-Contreras, E. Collantes-Estévez, C. López-Medina, I. Arias-de la Rosa, N. Barbarroja, Decoding clinical and molecular pathways of liver dysfunction in psoriatic arthritis: Impact of cumulative methotrexate doses, Biomed. Pharmacother. 168 (2023) 115779, https://doi.org/10.1016/j.biopha.2023.115779.
[11] N. Barbarroja, C. López-Medina, A. Escudero-Contreras, I. Arias-de la Rosa, Clinical and molecular insights into cardiovascular disease in psoriatic patients and the potential protective role of apremilast, Front. Immunol. 15 (2024) 1459185, https://doi.org/10.3389/fimmu.2024.1459185.
[12] I. Arias de la Rosa, M.D. López-Montilla, C. Román-Rodríguez, C. Pérez-Sánchez, I. Gómez-García, C. López-Medina, M.L. Ladehesa-Pineda, M.D.C. Ábalos-Aguilera, D. Ruiz, A.M. Patiño-Trives, M. Luque-Tévar, I. Añón-Oñate, M.J. Pérez-Galán, R. Guzmán-Ruiz, M.M. Malagón, C. López-Pedrera, A. Escudero-Contreras, E. Collantes-Estévez, N. Barbarroja, The clinical and molecular cardiometabolic fingerprint of an exploratory psoriatic arthritis cohort is associated with the disease activity and differentially modulated by methotrexate and apremilast, J. Intern. Med. 291 (5) (2022) 676–693, https://doi.org/10.1111/joim.13447.
[13] W. Taylor, D. Gladman, P. Helliwell, A. Marchesoni, P. Mease, H. Mielants, CASPAR Study Group, Classification criteria for psoriatic arthritis: development of new criteria from a large international study, Arthritis Rheum. 54 (8) (2006) 2665–2673, https://doi.org/10.1002/art.21972.
[14] M.M. Schoels, D. Aletaha, F. Alasti, et al., Disease activity in psoriatic arthritis (PsA): de ning remission and treatment success using the DAPSA score, Ann. Rheum. Dis. 75 (2016) 811–818.
[15] Expert Panel on Detection, Evaluation, and Treatment of High Blood Cholesterol in Adults, Executive summary of the third report of the national cholesterol education program (NCEP) expert panel on detection, evaluation, and treatment of high blood cholesterol in adults (Adult Treatment Panel III), JAMA 285 (19) (2001) 2486–2497, https://doi.org/10.1001/jama.285.19.2486.
[16] P.C. Chao, Y. Li, C.H. Chang, J.P. Shieh, J.T. Cheng, K.C. Cheng, Investigation of insulin resistance in the popularly used four rat models of type-2 diabetes, Biomed. Pharmacother. 101 (2018) 155–161, https://doi.org/10.1016/j.biopha.2018.02.084.
[17] C.B. Campanholo, A. Maharaj, N. Corp, S. Bell, L. Costa, K. de Vlam, N.J. Gullick, M. Khraishi, M. Kishimoto, N. Palmou-Fontana, S. Reddy, R. Scarpa, L. Vega, V. G. Duarte, D. Zisman, D. van der Windt, M.Y. Duruoz, Management of psoriatic arthritis in patients with comorbidities: an updated literature review informing the 2021 GRAPPA treatment recommendations, J. Rheuma 50 (3) (2023) 426–432, https://doi.org/10.3899/jrheum.220310.
[18] M.L. Boland, D. Oró, K.S. Tølbøl, S.T. Thrane, J.C. Nielsen, T.S. Cohen, D.E. Tabor, F. Fernandes, A. Tovchigrechko, S.S. Veidal, P. Warrener, B.R. Sellman, J. Jelsing, M. Feigh, N. Vrang, J.L. Trevaskis, H.H. Hansen, Towards a standard diet-induced and biopsy-confirmed mouse model of non-alcoholic steatohepatitis: impact of dietary fat source, World J. Gastroenterol. 25 (33) (2019) 4904–4920, https://doi.org/10.3748/wjg.v25.i33.4904.
[19] B. Wang, X. Zhu, S. Yu, H. Xue, L. Deng, Y. Zhang, Y. Zhang, Y. Liu, Roflumilast ameliorates GAN diet-induced non-alcoholic fatty liver disease by reducing hepatic steatosis and fibrosis in ob/ob mice, Biochem. Biophys. Res. Commun. 722 (2024) 150170, https://doi.org/10.1016/j.bbrc.2024.150170.
[20] Y. Wu, Y. Ma, CCL2-CCR2 signaling axis in obesity and metabolic diseases, J. Cell. Physiol. 239 (4) (2024), https://doi.org/10.1002/jcp.31192.
[21] L. Xu, Y. Chen, M. Nagashimada, Y. Ni, F. Zhuge, G. Chen, H. Li, T. Pan, T. Yamashita, N. Mukaida, S. Kaneko, T. Ota, N. Nagata, C C chemokine ligand 3 deficiency ameliorates diet-induced steatohepatitis by regulating liver macrophage recruitment and M1/M2 status in mice, Metabolism 125 (2021) 154914, https://doi.org/10.1016/j.metabol.2021.154914.
[22] L.G. Lorentzen, K. Yeung, N. Eldrup, J.P. Eiberg, H.H. Sillesen, M.J. Davies, Proteomic analysis of the extracellular matrix of human atherosclerotic plaques shows marked changes between plaque types, Matrix Biol. 21 (2024) 100141, https://doi.org/10.1016/j.mbplus.2024.100141.
[23] R. Bende, D. Heredea, I. Rațiu, I. Sporea, M. Dănilă, R. Șirli, A. Popescu, F. Bende, Association between visceral adiposity and the prediction of hepatic steatosis and fibrosis in patients with metabolic dysfunction-associated steatotic liver disease (MASLD), J. Clin. Med. 14 (10) (2025) 3405, https://doi.org/10.3390/jcm14103405.
[24] M.M. Murata, X. Kong, E. Moncada, Y. Chen, H. Imamura, P. Wang, M.W. Berns, K. Yokomori, M.A. Digman, NAD+ consumption by PARP1 in response to DNA damage triggers metabolic shift critical for damaged cell survival, Mol. Biol. Cell 30 (20) (2019) 2584–2597, https://doi.org/10.1091/mbc.e18-10-0650.
[25] S. Hara, H. Kono, N. Suto, H. Kojima, K. Kishimoto, H. Yoshino, S. Niiyama, Y. Kakihana, H. Ichinose, Inhibition of QDPR synergistically modulates intracellular tetrahydrobiopterin profiles in cooperation with methotrexate, Biochem. Biophys. Res. Commun. 717 (2024) 150059, https://doi.org/10.1016/j.bbrc.2024.150059.
[26] V. Murahovschi, O. Pivovarova, I. Ilkavets, R.M. Dmitrieva, S. Döcke, F. Keyhani-Nejad, Ö. Gögebakan, M. Osterhoff, M. Kemper, S. Hornemann, M. Markova, N. Klöting, M. Stockmann, M.O. Weickert, V. Lamounier-Zepter, P. Neuhaus, A. Konradi, S. Dooley, C. von Loeffelholz, M. Blüher, N. Rudovich, WISP1 is a novel adipokine linked to inflammation in obesity, Diabetes 64 (3) (2015) 856–866, https://doi.org/10.2337/db14-0444.
[27] D. Ngo, M.D. Benson, J.Z. Long, Z.Z. Chen, R. Wang, A.K. Nath, M.J. Keyes, D. Shen, S. Sinha, E. Kuhn, J.E. Morningstar, X. Shi, B.D. Peterson, C. Chan, D. H. Katz, U.A. Tahir, L.A. Farrell, O. Melander, J.D. Mosley, S.A. Carr, R.E. Gerszten, Proteomic profiling reveals biomarkers and pathways in type 2 diabetes risk, JCI Insight 6 (5) (2021) e144392, https://doi.org/10.1172/jci.insight.144392.
[28] K. Wilhelm, K. Happel, G. Eelen, S. Schoors, M.F. Oellerich, R. Lim, B. Zimmermann, I.M. Aspalter, C.A. Franco, T. Boettger, T. Braun, M. Fruttiger, K. Rajewsky, C. Keller, J.C. Brüning, H. Gerhardt, P. Carmeliet, M. Potente, FOXO1 couples metabolic activity and growth state in the vascular endothelium, Nature 529 (7585) (2016) 216–220, https://doi.org/10.1038/nature16498.
[29] Q. Pan, M. Gao, D. Kim, W. Ai, W. Yang, W. Jiang, W. Brashear, Y. Dai, S. Li, Y. Sun, Y. Qi, S. Guo, Hepatocyte FoxO1 deficiency protects from liver fibrosis via reducing inflammation and TGF-β1-mediated HSC activation, Cell. Mol. Gastroenterol. Hepatol. 17 (1) (2024) 41–58, https://doi.org/10.1016/j.jcmgh.2023.08.013.
[30] F. Norheim, K. Chella Krishnan, T. Bjellaas, L. Vergnes, C. Pan, B.W. Parks, Y. Meng, J. Lang, J.A. Ward, K. Reue, M. Mehrabian, T.E. Gundersen, M. Péterfy, K. T. Dalen, C.A. Drevon, S.T. Hui, A.J. Lusis, M.M. Seldin, Genetic regulation of liver lipids in a mouse model of insulin resistance and hepatic steatosis, Mol. Syst. Biol. 17 (1) (2021) e9684, https://doi.org/10.15252/msb.20209684.